(Received 3 September 2024, Accepted 17 October 2024, Scheduled 25 October 2024)

Design of X-Band Vertical Non-Standard Coaxial-Waveguide Converter

Bo Yan[1,*], Zibin Weng[1,2], Dalei Yuan[1], and Youqian Su[1]

[1] *Hangzhou Institute of Technology, Xidian University, Hangzhou 311231, Zhejiang, China*
[2] *National Key Laboratory of Radar Detection and Sensing, Xidian University, Xi'an 710071, Shaanxi, China*

ABSTRACT: A non-standard rectangular waveguide-to-coaxial converter designed for the X-band (9.3–9.5 GHz) is presented. This converter builds upon traditional coaxial probe coupling and stepped contact feeds by integrating a Chebyshev impedance transformer and stepped impedance matching technique. The proposed improved converter features a coupling probe combined with a stepped contact, enabling a vertical feed configuration from the bottom. This design offers an effective option for optimizing array antenna layouts. Simulation results indicate that within the operational frequency range, the rectangular waveguide-to-coaxial converter achieves $|S_{11}|$ less than -27 dB and $|S_{21}|$ greater than -0.04 dB. Practical measurements for non-standard rectangular waveguides show a VSWR below 1.1 across the working frequency band.

1. INTRODUCTION

The coaxial-waveguide converters are widely used in microwave systems for radar, communication, satellites, and electronic warfare, serving as crucial passive connecting components for signal transmission and signal processing in radar, communication, and microwave testing systems [1–3]. The design of coaxial-waveguide converters encompasses various factors, including feeding methods, structure, and dimensions. Notably, choosing an appropriate feeding method has a significant impact on the cascading of antenna systems [4–7]. Ref. [8] proposes an adaptor for matching standard coaxial lines to a reduced-height rectangular waveguide for the C-band, utilizing a wide face center probe coupling feeding method. Ref. [9] presents a simulation-based design methodology for a broadband transition from coaxial cable to rectangular waveguide. This transition features a coaxial probe linked to either a cylindrical head or a disk, along with two symmetrically positioned tuning posts, employing three sections of rectangular waveguide with appropriately selected dimensions, clearly belonging to the wide face center probe coupling feeding category. Ref. [10] introduces a computational design approach for a broadband online coaxial to rectangular waveguide transition with a bandwidth of $2.83:1$, consisting of a fourth-order ridge transformer and three sections of rectangular waveguide, fed by a coaxial probe connected from the side. Ref. [11] outlines a design methodology for a Ka-band waveguide coaxial transformer based on a single-ridge waveguide impedance transformer, where feeding is chosen to extend coaxially inward from the wide face to connect with a stepped impedance feed. Ref. [12] proposes a linear transition operating in the Q-band between coaxial cables and rectangular waveguides. Ref. [13] introduces, for the first time in the X-band, a transition from coaxial to groove gap waveguide, addressing the lack of similar designs in recent literature. Refs. [8, 9, 11] pertain to vertical wide face feeding methods, using coaxial probes to connect with thick probes or simultaneously adding matching steps to position the probes at the maximum electric field strength, with directions parallel to the field, resulting in a simple structure capable of achieving good feeding. However, since feeding occurs on the wide face, it does not affect single antenna feeding, but may impact structural arrangement when cascading antenna arrays. Refs. [10, 12, 13] involve back feeding methods through probes contacting matched impedance steps, or spaced appropriately from the back end of the steps for narrow face feeding at the rear side of the rectangular waveguide, which does not affect the spacing between array elements. This allows phased array antennas to achieve larger scanning angles. However, when the antenna size is constrained, adding feeding at one end may increase the antenna size, affecting system cascading.

As application demands become more specific, the uniqueness of antenna models and the design of waveguide-to-coaxial converters for particular scenarios gain increasing importance. Taking the waveguide slot array antenna commonly used in radar systems as an example, the design of coaxial-to-waveguide converters tailored to the array antenna configuration and the overall system construction is crucial. For instance, Figure 1(a) illustrates a traditional vertical converter, where the thick probe can be removed. Due to the longer wide edge, the array spacing will increase, reducing the theoretical maximum scan angle and leading to grating lobes in the antenna radiation pattern. Conversely, Figure 1(b) shows a back-fed converters, where most current feeding methods involve contacting the narrow face with a coaxial probe or feeding from an appropriate distance from the steps. This approach maintains bandwidth while minimally affecting

* Corresponding author: Bo Yan (1401132184@qq.com).

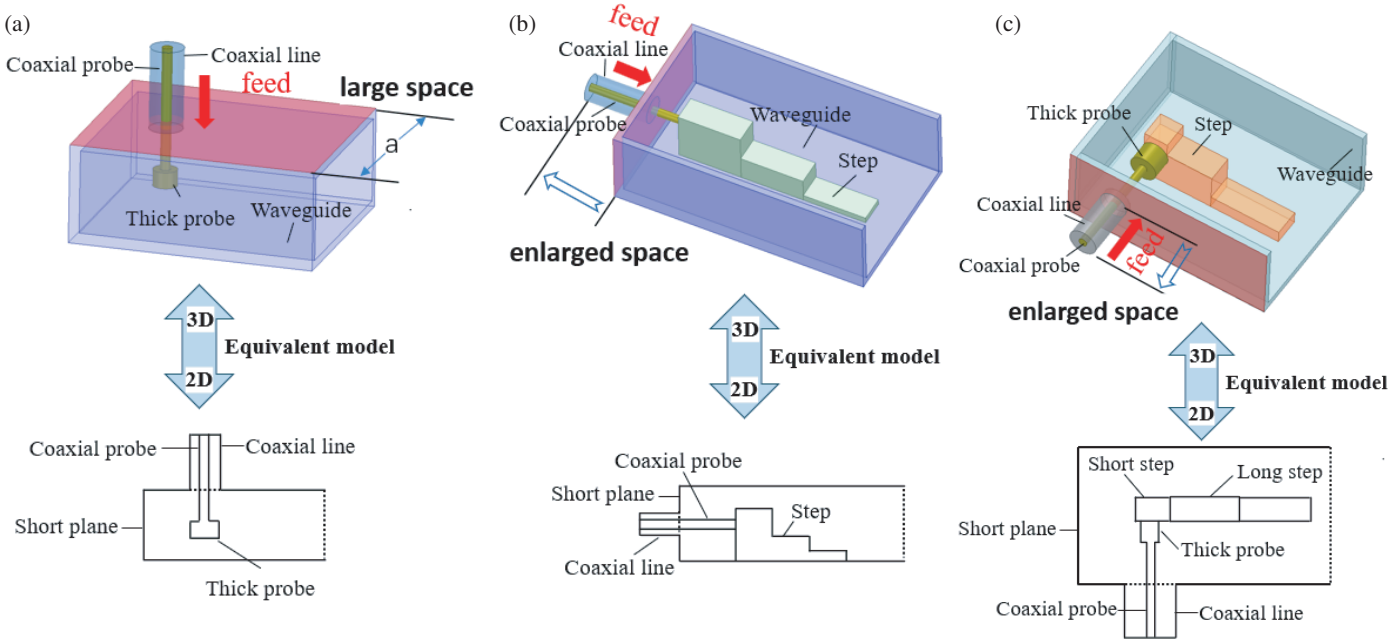

FIGURE 1. Coaxial-waveguide converter structure. (a) Vertical converter. (b) Feed-back converter. (c) Modified converter.

the array antenna spacing and achieving low loss, albeit with some increase in overall dimensions. This paper proposes an improvement to the traditional vertical feeding method by using a non-standard rectangular waveguide. The original wide-face vertical feeding is replaced with narrow-face bottom vertical feeding, incorporating steps and thick probes as shown in Figure 1(c). By feeding through the narrow face at the bottom of the rectangular waveguide, the feeding position is shifted from the wide-face center or narrow-face rear end to the narrow-face bottom. This modification achieves good performance in terms of standing wave and insertion loss without altering the dimensions at both ends of the antenna. The design provides a new feeding position and structure that does not affect the parallel array configuration of the antenna.

2. THEORY ANALYSIS

This paper presents a design for a non-standard flat rectangular waveguide to coaxial converter, significantly reducing the dimensions of the narrow side based on the standard waveguide WR-90. This converter is developed utilizing the theoretical framework of quarter-wavelength impedance transformers and Chebyshev multi-section matching transformers, incorporating structural improvements in its design. It consists of four main components: a metal probe with coaxial dielectric, a metal step, and a waveguide cavity. The metal probe is constructed from a combination of a thin probe and a thick probe; the coaxial dielectric is made of Teflon, while both the metal step and the cavity are fabricated from aluminum.

In the design process, given the passband ripple ρ_r, relative bandwidth W_q, and impedance ratio R of the two terminals, formula (1) can be used to determine M. Ref. [14] provides the relationship between M and W_q and n, with M given by:

$$M\left(n, W_q\right) = T_n^2\left(\frac{1}{\mu_0}\right) = \frac{\varepsilon_a}{\varepsilon_r} = \frac{\frac{(R-1)^2}{4R}}{\frac{(\rho_r-1)^2}{4\rho_r}} \tag{1}$$

Based on the computed range of M, the appropriate value of n can be determined. If the computed M does not fall within the tabulated range, adjustments to ρ_r or W_q should be made to ensure that the calculated M remains within a reasonable range.

Additionally, for a quarter-wavelength step transformer as shown in Figure 2, different values of n correspond to the calculation formulas (2)–(4):

$$\text{For } n = 2,\ Z_2{=}R/Z_1 \tag{2}$$

$$\text{For } n = 3,\ Z_2 = \sqrt{R},\ Z_3 = R/Z_1 \tag{3}$$

$$\text{For } n = 4,\ Z_3 = R/Z_2,\ Z_4 = R/Z_1 \tag{4}$$

By consulting [15, 16], the normalized impedance values Z_1 for step numbers $n = 2$ and $n = 3$ can be obtained. Additionally, for $n = 4$, the normalized impedance values Z_1 and Z_2 can be determined.

Based on Chebyshev impedance transformation theory and step transformer theory, a model for a planar coaxial waveguide converter is proposed, as illustrated in Figure 3, with specific parameter values provided in Table 1. Panel (a) depicts the main body of the model, while panels (b), (c), and (d) show the front view, right view, and rear view, respectively.

The cavity model is made of aluminum with dimensions: length L, width b, and height a. The left-side reflective surface of the cavity is denoted by W_d and has a wall thickness of W_T. The bottom of the cavity consists of a rectangular aluminum metal plate that includes a coaxial cable and has the same width

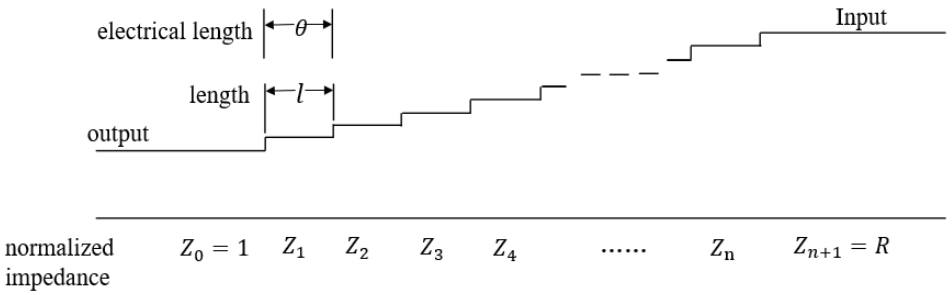

FIGURE 2. Quarter-wavelength step-converter.

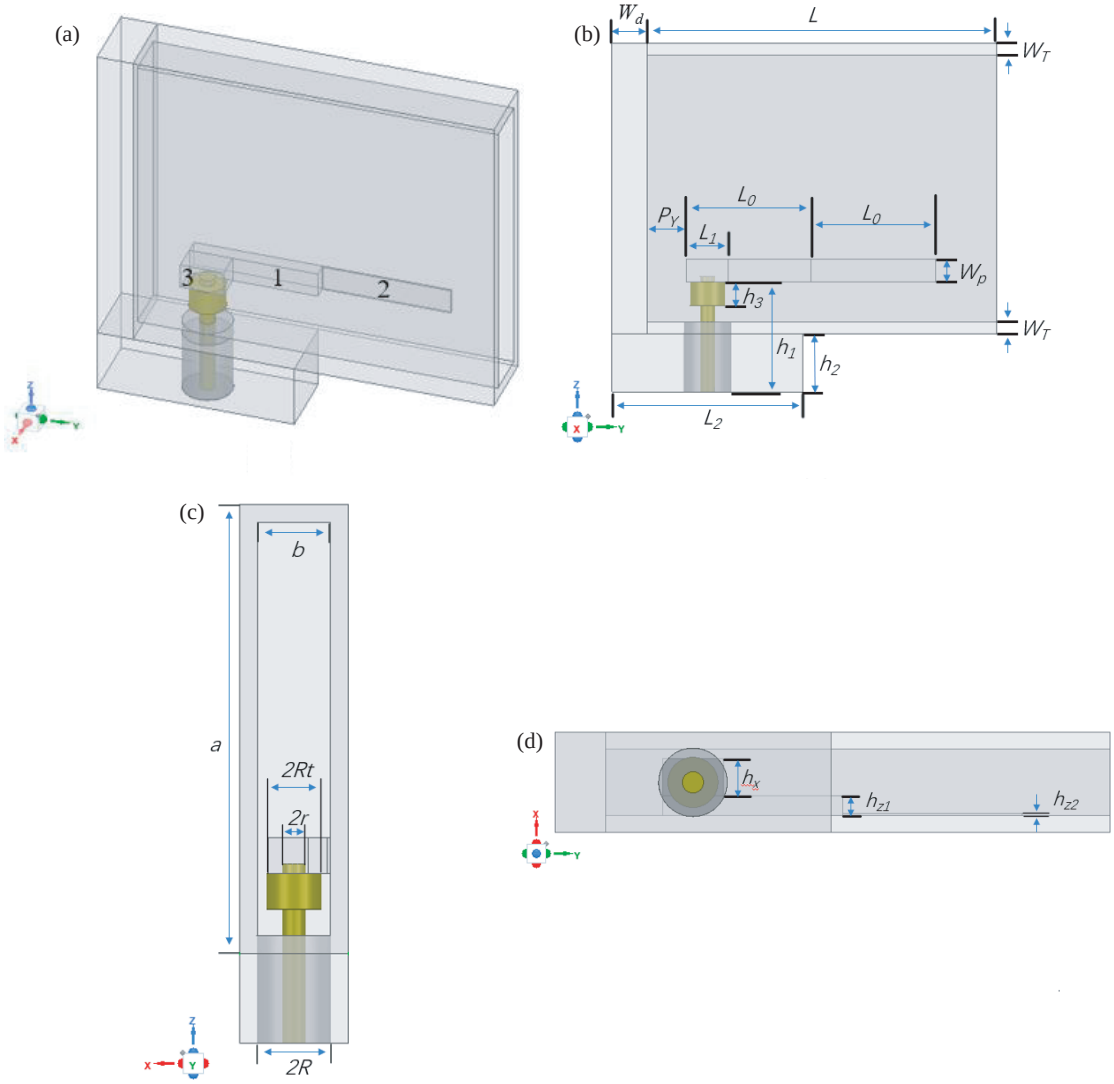

FIGURE 3. The model and specific dimension. (a) Overall structure of the model. (b) Front of the model and specific dimensions. (c) Right side of the model and specific dimensions. (d) Bottom of the model and specific dimensions.

as the cavity, with length L_2 and width h_2. The inner surface of the cavity features stepped structures made of aluminum, as shown in Figure 3(a). There are three steps labeled 1, 2, and 3, with lengths L_0, L_0, and L_1, and heights h_{z1}, h_{z2}, and h_x, respectively, while the width is W_p.

Ignoring step 3 and considering $n = 2$, the normalized impedance values for steps 1 and 2 are 1.81407 and 5.8045, respectively. The height of each step is calculated using the formula:

$$h_i = \frac{b\lambda}{240\pi\lambda_g} \cdot Z_i \quad (i = 1, 2) \tag{5}$$

where λ is the wavelength, and λ_g is the guided wavelength. Optimization yields the heights h_{z1} and h_{z2} for steps 1 and 2, respectively.

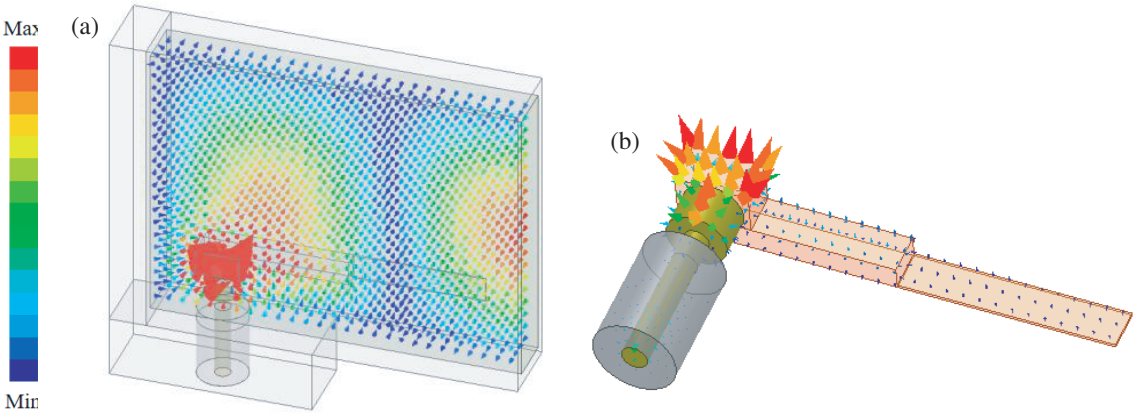

FIGURE 4. Voltage distribution. (a) Voltage distribution diagram in the air cavity. (b) Voltage distribution diagram of step and surrounding cavity excitation.

TABLE 1. Specific data of model parameters.

a	b	W_T	W_d	P_Y	W_p	L
22.86	4	1	3	5.2	2	30
L_0	L_1	L_2	h_1	h_2	h_3	R_t
10.7	3.6	16.4	9.4	4.97	2	1.5
R	r	h_x	h_{z1}	h_{z2}		
2.05	0.635	2.2	1.2	0.14		

Unit: mm

When the coaxial probe extends into the cavity, the dielectric surrounding the inner conductor transitions from Teflon to air, resulting in a change in the wave conduction medium. Consequently, the propagation mode of the wave shifts from the original TEM mode to higher-order modes. The device operates with the wide and narrow sides in the X-band, satisfying the conditions for single-mode transmission; thus, the higher-order mode within the rectangular cavity is the TE10 mode.

Simultaneously, the impedance of the coaxial probe that extends into the cavity also changes. Within the coaxial line, the characteristic impedance is 50 Ω, and as the length of the inner conductor extending into the cavity increases, the end face's reactance also increases. To counteract the inductance introduced by the fine coaxial probe, a thick probe is incorporated to increase capacitance.

Consequently, the coaxial probe is composed of two parts: the section adjacent to the step is the thick probe, with a radius R_t and a length h_3. The longer section is the coaxial probe, with a radius r and a length $h_1 - h_3$, in addition to a portion that extends into the step, measuring 0.5 mm in length. The radius of the coaxial dielectric is denoted as R.

The normalized impedance value of step 3 cannot be validated using the quarter-wavelength impedance transformation theory. Voltage and current field distributions are illustrated in Figure 6. As seen in Figure 4(a), step 3 and the thick probe excite the TE10 mode. Specifically, step 3 and the wide surface of the cavity form a local surface capacitance. The capacitance can be calculated using formula (6):

$$C = \frac{\varepsilon S}{d} \tag{6}$$

where ε is the dielectric constant of air, S the area of the upper surface of step 3, and d the distance between the upper surface of step 3 and the wide surface of the cavity. It can be observed that when the distance d is very small, the capacitance value is very high. To clearly depict the voltage and current distributions, the cavity is omitted from the following distribution diagrams. Figure 4(b) shows that the voltage is maximized at step 3.

The surface capacitance formed by steps 1, 3, the thick probe, and the cavity enhances the local current excitation. Figure 5 illustrates the current distribution clearly. To better visualize the current distribution, Figure 5(a) depicts the main current distribution with the cavity omitted. Figure 5(b) shows that, in the small loop, a surface capacitance is formed between the thick probe and the opposing surface. The current flows along the cavity surface to the probe surface and then radiates to the opposite surface, forming a current loop. In the large loop, the current flows from the lower wide surface of the cavity to the step, then from step 3 to the upper wide surface of the cavity, and finally returns to the lower wide surface of the cavity, forming a complete loop. Figures 5(c) and 5(d) provide similar analysis as shown in Figure 5(b).

The photograph of the fabricated device is shown in Figure 6. During measurement, the two waveguides were joined for testing. The simulated and measured $|S_{11}|$ and $|S_{21}|$ are as follows.

Based on the analysis of Figure 6, the measured and simulated $|S_{11}|$ values within the frequency band of 9.2–9.6 GHz show a general agreement, although some discrepancies exist between the numerical values. The measured $|S_{11}|$ in the operational frequency range of 9.3–9.5 GHz is less than -20 dB. The simulated $|S_{21}|$ values present a curve very close to 0 dB, with a maximum value of approximately -0.04 dB; conversely, the measured $|S_{21}|$ exhibits a fluctuating curve within -0.5 dB across the 9.2–9.6 GHz range, reaching about -1 dB at 9.2 GHz. There are notable differences in the waveforms of the simulated and measured $|S_{21}|$.

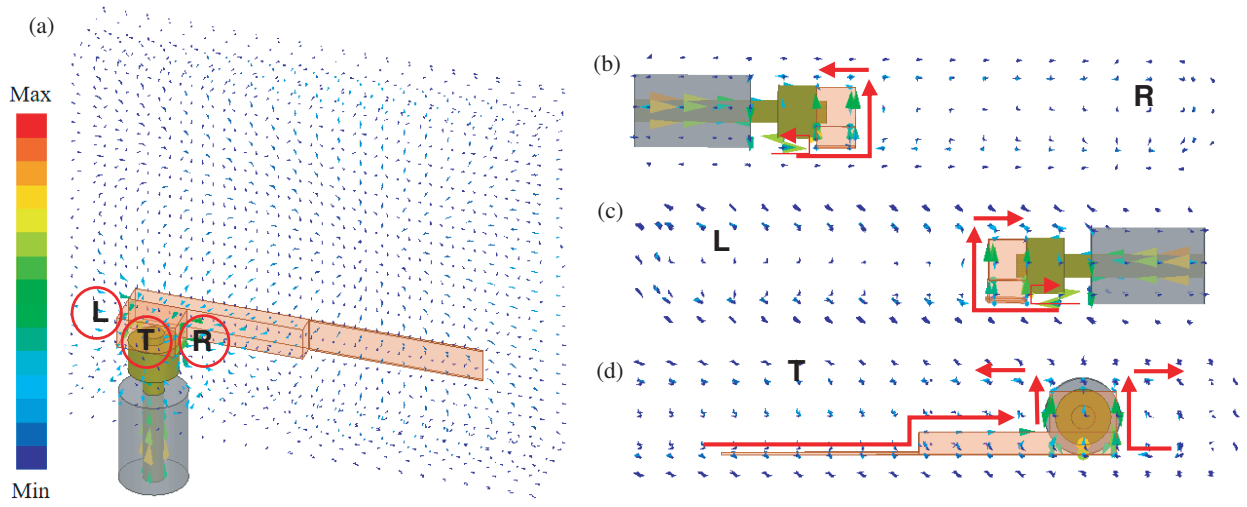

FIGURE 5. Current distribution. (a) The main body current distribution. (b) The loop current distribution with the right chamber step. (c) The loop current distribution with the left chamber step. (d) The loop current distribution with the top cavity surface.

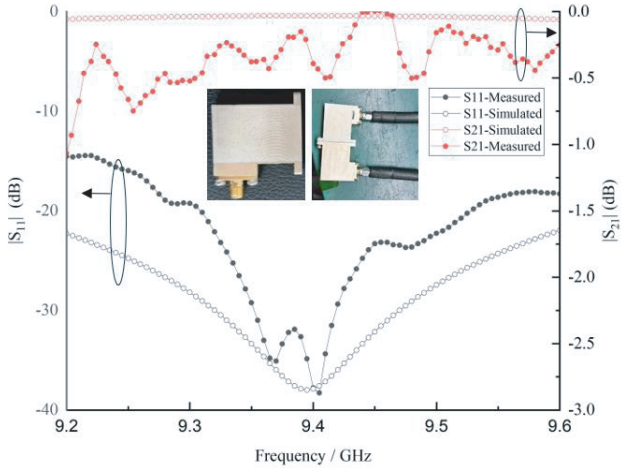

FIGURE 6. S_{11} and S_{21} between simulation and measurement and physical picture.

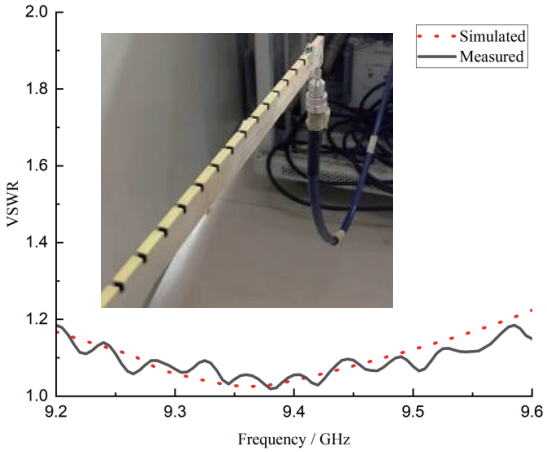

FIGURE 7. Simulation of a non-standard waveguide VSWR and physical picture.

Upon analysis, during the simulation using HFSS software, the two ports were configured as ideal wave ports, yielding results based on the simulation of a single waveguide-to-coaxial converter. In contrast, for the testing phase, to simulate matched conditions at both ports, another waveguide-to-coaxial converter was directly connected, representing an equivalent 50-ohm load. However, in practice, achieving perfect 50-ohm matching between the two ports is not feasible. Additionally, the connection is made through flanges that introduce a gap between the two waveguide-to-coaxial converters, resulting in discontinuity on the inner cavity surface, leading to impedance variations and subsequent reflected waves. This causes discrepancies in the obtained $|S_{11}|$ and $|S_{21}|$ measurements. Furthermore, the design of the waveguide-to-coaxial converter was centered around a frequency of 9.4 GHz; deviations from this center frequency result in poorer impedance matching, particularly evident at the edges of the frequency band where the $|S_{11}|$ results are suboptimal.

In summary, although the results exhibit some deviation from the simulated outcomes, the measured results meet the performance requirements. Thus, the waveguide-to-coaxial converter can be deemed relatively successful. To validate its practical application, we connected the waveguide-to-coaxial adapter to a non-standard coaxial converter for further testing, as shown in Figure 7.

In Figure 7, the photograph depicts the designed coaxial waveguide converter connected to a non-standard rectangular waveguide with a length of 2418 mm. Due to the length of the physical model, only the corresponding feeding section is shown. It can be observed that within the frequency range of 9.2 to 9.6 GHz, the simulated and measured results of the Voltage Standing Wave Ratio (VSWR) align closely, with the measured VSWR being less than 1.2; within the range of 9.3 to 9.5 GHz, the VSWR is less than 1.1. Therefore, this design demonstrates good performance within the operating frequency band, meeting the engineering requirements.

3. CONCLUSION

This paper investigates a non-standard rectangular waveguide-to-coaxial converter, based on the Chebyshev step impedance matching theory. By incorporating matching blocks and coarse probes, and optimizing the corresponding dimensions and positions, good impedance matching was achieved. The feasibility of the design concept was validated through simulations. After fabricating the physical prototype and conducting tests, the results indicated that within the frequency range of 9.3–9.5 GHz, the simulated $|S_{11}|$ is less than -27 dB, while the measured $|S_{11}|$ is below -20 dB. The simulated $|S_{21}|$ results are within -0.04 dB, whereas the measured results fluctuate around -0.5 dB.

The primary reason for the discrepancies between ideal simulations and actual test results can be attributed to the differences in the measurement setup. During simulation, an ideal model of a single waveguide-to-coaxial converter was considered; however, during testing, two waveguide-to-coaxial converters were connected, resulting in a gap between them and incomplete impedance matching at the two ports. To assess the performance of the converter, a non-standard rectangular waveguide was terminated, revealing a voltage standing wave ratio (VSWR) of less than 1.1 within the operational frequency band, indicating satisfactory performance. This work provides insights for the design of waveguide-to-coaxial converters. Future research may focus on broadening the frequency range and enhancing performance stability.

REFERENCES

[1] Bharath, K., S. V. Nandigama, D. Ramakrishna, and V. M. Pandharipande, "High performance millimeter wave SIW slotted array antenna," *Progress In Electromagnetics Research C*, Vol. 125, 15–23, 2022.

[2] Masouleh, M. S., A. K. Behbahami, M. S. Masouleh, M. Sajedi, and M. Adjouadi, "Pattern synthesis of a resonant slot on a broad wall of the rectangular waveguide using amplitude and phase control," *Progress In Electromagnetics Research C*, Vol. 129, 51–61, 2023.

[3] Yu, W., L. Sun, L. Li, and H. Sun, "Dual-band dual-polarized slotted coaxial waveguide antenna," *Progress In Electromagnetics Research C*, Vol. 120, 135–144, 2022.

[4] Simion, S., "A new unterminating method for de-embedding the coaxial to waveguide transitions," *Progress In Electromagnetics Research C*, Vol. 121, 255–264, 2022.

[5] Haider, I., A. Basu, and S. K. Koul, "A compact wideband waveguide filtering antenna with transmission zero," *Progress In Electromagnetics Research Letters*, Vol. 119, 59–65, 2024.

[6] Nesterenko, M., V. A. Katrich, S. V. Pshenichnaya, and V. I. Kijko, "Scattering of electromagnetic waves by a multi-element system of pass-through resonators in a rectangular waveguide," *Progress In Electromagnetics Research C*, Vol. 131, 135–143, 2023.

[7] Tribak, A., J. Zbitou, A. M. Sanchez, and N. A. Touhami, "Ultra-broadband high efficiency mode converter," *Progress In Electromagnetics Research C*, Vol. 36, 145–158, 2013.

[8] Komarov, V. V., A. I. Korchagin, and V. P. Meschanov, "Broadband coaxial-to-waveguide transition," in *2020 International Conference on Actual Problems of Electron Devices Engineering (APEDE)*, 163–165, Saratov, Russia, 2020.

[9] Dansran, B., S. Xu, J. Heo, C.-S. Lee, and B.-C. Ahn, "Design of a broadband transition from a coaxial cable to a reduced-height rectangular waveguide," *Applied Sciences*, Vol. 13, No. 20, 11265, 2023.

[10] Zhang, Q., S. Xu, J. Heo, E. Altanzaya, G.-Y. Ariunbold, D. Otgonbat, C.-S. Lee, B.-C. Ahn, S. Li, and S.-G. Choi, "Computational design of a broadband in-line coaxial-to-rectangular waveguide transition," *Applied Sciences*, Vol. 14, No. 1, 74, 2024.

[11] Huang, Y. Q. and C. A. Liu, "Waveguide-coaxial converter based on single-ridge waveguide impedance transformation in Ka band," in *2020 3rd International Conference on Electron Device and Mechanical Engineering (ICEDME)*, 78–81, Suzhou, China, 2020.

[12] Simone, M., A. Fanti, M. B. Lodi, T. Pisanu, and G. Mazzarella, "An in-line coaxial-to-waveguide transition for Q-band single-feed-per-beam antenna systems," *Applied Sciences*, Vol. 11, No. 6, 2524, 2021.

[13] Rossi, R. and R. V. Gatti, "X-band in-line coaxial-to-groove gap waveguide transition," *Electronics*, Vol. 11, No. 15, 2361, 2022.

[14] Young, L., "Stepped-impedance transformers and filter prototypes," *IRE Transactions on Microwave Theory and Techniques*, Vol. 10, No. 5, 339–359, Sep. 1962.

[15] Young, L., "Tables for cascaded homogeneous quarter-wave transformers," *IRE Transactions on Microwave Theory and Techniques*, Vol. 7, No. 2, 233–237, Apr. 1959.

[16] Cohn, S. B., "Optimum design of stepped transmission-line transformers," *IRE Transactions on Microwave Theory and Techniques*, Vol. 3, No. 3, 16–20, Apr. 1955.